Unsteady Flow around an Exposed Rotating Wheel

Author:
Ramachandran, Darshillan; Doig, G.C.

Event details:
AIAA Region VII-AU Student Conference
Adelaide, Australia

Publication Date:
2012

DOI:
https://doi.org/10.26190/unsworks/40

Unsteady Flow around an Exposed Rotating Wheel

D.Ramachandran* G.C Doig†

School of Mechanical and Manufacturing Engineering, University of New South Wales,Sydney,NSW,2052,Australia

The flow around an exposed rotating wheel, such as those on a Formula 1 car, is complex in nature; experimental investigation using wind tunnel is expensive and may not be able to show intricate flow features. Computational Fluid Dynamics (CFD) can enable numerical solutions of flow over an exposed wheel, but due to issues of computational cost only steady-state Reynolds Averaged Navier Stokes (RANS) methods are commonly used. In the present work, an exposed rotating wheel in contact with a moving ground was modeled using unsteady RANS, Large Eddy Simulation (LES) and Detached Eddy Simulation (DES). These transient methods demonstrate more intricate details of the flow not seen in steady state simulations. In addition, LES and DES more accurately resolves the large scale eddies that will be apparent especially in the wheel wake and enable the flow field to be understood in a more complete way.

I. Nomenclature

d	=	wheel diameter
C_p	=	pressure coefficient
C_D	=	drag coefficient
C_L	=	lift coefficient
x	=	positive direction of air flow
CFD	=	Computational Fluid Dynamics
RANS	=	Reynolds-Averaged Navier Stokes
sRANS	=	steady-state RANS
URANS	=	unsteady RANS
LES	=	Large Eddy Simulation
DES	=	Detached Eddy Simulation
WALE	=	Wall-Adapting Local Eddy-Viscosity
SGS	=	sub-grid scale
FFT	=	Fast Fourier Transform
$\|H\|$	=	Magnitude of the frequency spectrum

II. Introduction

The flow around an exposed rotating wheel is very complex and unsteady in nature. An exposed rotating wheel is an integral part of the motorsport industry like Formula 1 (F1). The amount of drag induced by the wheel has been quantified to be about 40% of the total drag in a F1 car.[1] However, the flow features associated with an exposed rotating wheel are still currently not well understood for a number of reasons. Experimental study carried out in the late 1960s and early 1970s used a wind tunnel balance or load cells to measure aerodynamic forces acting on a wheel but interference from unknown and variable contact forces between the wheel and the ground prohibited accurate measurement to be taken.[2]The benchmark experiment study on this field was done by Fackrell employing the use of a moving ground with a wheel in constant contact. Aerodynamic forces were obtained by integrating the static surface pressures which were electronically measured.[3] Fackrell tested six different wheel shapes that were representative of the tyres and rim used on a Formula 1 car at that time, consisting of three tread width with two

* Undergraduate student, School of Mechanical and Manufacturing Engineering, University of New South Wales (UNSW), Student Member AIAA

† Associate Lecturer, School of Mechanical and Manufacturing Engineering, University of New South Wales (UNSW), Member AIAA.

different edge profiles. All wheels shared the same diameter, d=416mm and were made of aluminium alloy. The wheels designated "A", "B" and "C" has a tread width of 0.46d, 0.61d and 0.81d, respectively. The two edge profiles were labeled as "1" and "2". The experiments carried out by Fackrell proved the importance of conducting the experiment with the wheel in contact with a moving ground because he was able to prove that such a wheel is a lifting body and not a downforce generating component as predicted by other authors[11,12] that used the load balance method to derive aerodynamic forces. The reason a downforce was predicted by those authors was postulated to be due to the venturi effect that takes place when the wheel is slightly lifted off the ground surface at the contact patch[3]. In general, Fackrell's experiments accurately quantified flow features that had only previously been observed or assumed - namely, that the flow stagnates at the front of the wheel where the air first arrives at the geometry, and air travelling over the top of the wheel separates completely while the remainder is pushed around the sides or down to the moving ground, where the flow is pushed out to the sides, having no other direction to travel in. Based on his experiments, Fackrell found some distinct variation in flow field features between the rotating wheel and the stationary wheel. He found a jetting flow feature to occur on the rotating wheel just adjacent to the contact patch that contributed to an elevated pressure in this region and hence more lift. A pressure coefficient of greater than 1 was observed at the contact patch. In addition, based on Thom's [4] work, Fackrell, using mathematical proof was able to conclude that the separation over an exposed rotating wheel occurs adjacent to the wheel surface and not from the surface itself as observed from the stationary wheel.

Since the development of computational fluid dynamics (CFD) approaches to predict aerodynamic behaviours, several attempts to study the flow around an exposed wheel have been made. Axon[5] simulated the flow over an exposed rotating wheel with a geometry similar to that of Fackrell's "B2" wheel. Axon conducted a steady state RANS simulation using k-ε RNG two layer turbulence model. Axon was able to observe the jetting effect adjacent to the contact patch but his prediction in relation to the position of the separation point was off by about 30°.[5] Similarly, Diasinos[6] conducted extensive CFD validation study on Fackrell's "A2" wheel geometry. He obtained overall good predictions for surface pressure coefficient except a significant over prediction of pressure coefficient at the separation point for the rotating wheel. Diasinos' lift and drag coefficient matched that off Fackrell closely. Diasinos' study on the wheel wake shape of a rotating wheel by separating the boundaries of the wheel to allow rotation either at the top or the bottom half of the wheel allowed for him to conclude that the lift and drag is sensitive to the separation location. A more forward separation point resulted in lift and drag coefficient decreasing. An unsteady RANS (URANS) simulation method was done by McManus and Zhang[1]. They attempted the simulation on Fackrell's "A2" wheel geometry and were able to obtain good surface pressure, lift and drag forces correlation with the experimental set up. The authors concluded that for a rotating wheel, the flow separates near the top of the wheel and forms an arch shaped vortex. They also concluded that the Spalart Allmaras model was better at predicting surface pressures, separation position and pressure forces. The most recent development in the prediction of flow over an exposed rotating wheel using CFD was done by Salati[8] who did a Detached Eddy Simulation (DES) on Fackrell's "A2" wheel geometry to investigate the suitability of using this method to predict the flow over an exposed wheel. His work showed that DES was able to provide good surface static pressure correlation with Fackrell's experimental work[8]. Collectively, the work presented by Dassanayake *et al.*[13] concluded that DES was able to predict the arch-shaped vortex as per McManus and Zhang's URANS simulations, showed that the flow downstream the line of contact interacts with the vortices formed from the hub due to the rotation of the wheel and in general the DES was able to provide greater level of detail of the flow.

Since accurate experimental study on a wheel is extremely difficult[14] and due to inherently unsteady nature of the flow over an exposed rotating wheel[8,13], the focus of the present work is to investigate the complex flows over an exposed rotating wheel using unsteady RANS (URANS), Large Eddy Simulations (LES) and Detached Eddy Simulation (DES). Surface pressure comparison results were compared with Fackrell's experiments. The lift and drag cannot be directly compared because in the experiments, these quantities were derived by integrating the surface pressures using a unique approach to account for three-dimensionality, whereas, the simulation technique allows for direct computation of the lift and drag values. Some of the complex flow features are presented and discussed to provide greater insight into the flowfields predicted by the different simulation methods.

III. Description of Computational Model

A. Wheel geometry and Grid Description

The wheel geometry was modeled to be as accurate as possible to Fackrell's "A2" wheel geometry. The wheel has a diameter of 416mm and a width of 191mm. The cross section of the wheel is shown in Fig. 1. As shown in Fig.

1, the wheel geometry used by Fackrell had a lip between the wheel and the hubs. Upon initial investigation with steady-state solutions the lip was found to have minimal effect on the overall flow features. Yet, require an extremely fine mesh for definition. Therefore, for all results presented here, the wheel geometry used was the one without the lip hence there is a flat surface between the wheel and hubs. An important aspect of modeling the wheel in contact with the moving ground is the contact patch. In reality, a line contact is encountered but for the computational study this is not possible as a line contact will generate highly skewed cells. A region of volume needs to be modeled to represent the contact patch. In the present work, the contact patch was modeled based on Diasinos' work and was made to be 1.2mm high.

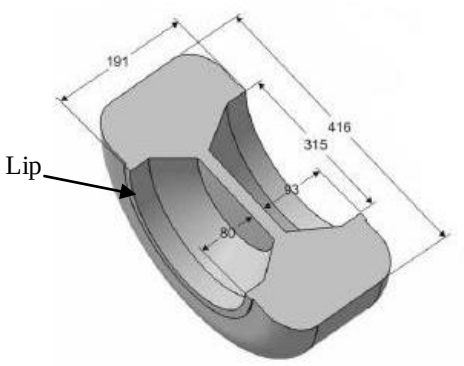

Figure 1. Section through Fackrell's "A2" wheel geometry

The wind tunnel domain was designed to be 20d = 8.3m long, 1.2m wide and 1.5m high in close correlation to the wind tunnel used in Imperial College London by Fackrell.[3] The wheel was placed in the middle of the domain. This was done to minimize the influence of the wheel's rotation at the inlet and to allow for more wheel wake features to be captured towards the outlet. The moving ground was modeled to be 5d=2.1m long on either side of the centre line of the wheel with the same width as the overall domain.

The grid was generated using the commercial software STAR-CCM+ by employing the trimmer meshing technique to generate the volume mesh. The trimmer meshing model utilizes a template mesh constructed from hexahedral cells from which it cuts or trims the core mesh based on the starting input surface.[7] Star CCM was used as it generates high-quality but efficient Cartesian background meshes with boundary layer prisms for capturing attached shear layers.[13] A cylindrical shaped volumetric control around the wheel and a rectangular shaped volumetric control at the wheel wake were set up to better capture the flow features in these regions. Two grids were generated; one labeled coarse mesh (3.48million cells) and the other labeled fine mesh (6.97million cells).

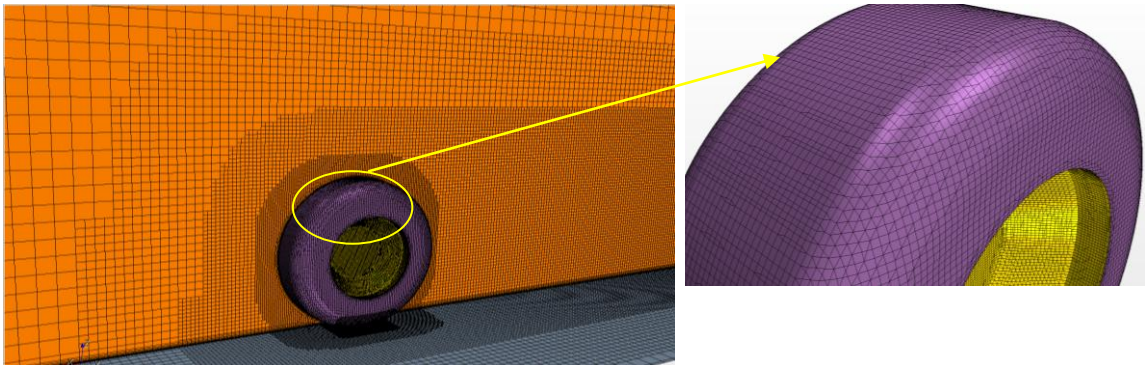

Figure 3. Computational grid on the wheel, moving ground and wake region (coarse mesh: 3.48 million cells). Detail view showing cartesian mesh on the wheel surface

A Grid Convergence Index (GCI) study was done based on results obtained from the LES to quantify the errors associated when using the coarse mesh compared to the fine mesh. Based on lift and drag coefficients the GCI was

found to be 1.7% and 2.7%, respectively. Therefore, only a small error is associated with the coarse mesh when the computational cost involved in running simulations using a finer mesh is factored in to considerations. Hence, all results presented in this paper are based on the coarse mesh solution. This grid has a y^+ value of less than 1 all around the wheel except at the interface between the wheel and the contact patch where a y^+ value of 2.7 was obtained.

B. Boundary Conditions

The boundary conditions were chosen to represent Fackrell's experimental set up as closely as possible, with the major exception that the hub where the sting attached to the wheel, for which no useful geometric details were available. The inlet velocity and moving ground speed were set to be 18.6m/s. The angular velocity of the wheel was set to be 89.4 rad/s which the equivalent of the linear moving ground speed of 18.6m/s based on the wheel diameter. This gives a Reynolds Number, Re= 5.3×10^5.

C. Numerical methods

The commercial code ANSYS FLUENT 13.0 was used to solve the problem to take advantage of available parallel computing resources at the Faculty of Engineering, UNSW. When employing the RANS approach, the predicted flow comprises the mean flow quantities, and a turbulence model is required to model turbulent flow behaviour. The URANS method is essentially the Reynolds-Averaged solutions method with the transient terms included in solving the governing equations. Unlike the RANS methods, LES resolves for most of the large scale eddies that are expected to occur in the wheel wake and only models, using a sub-grid scale (SGS) model, the small scale eddies. Finally, DES is a combination between LES and URANS. LES requires a very high resolution mesh in near-wall areas to correctly predict flow features in this region. Thus, DES was formulated so that in separated regions the LES formulation is used and in the boundary layer the unsteady RANS simulation method is invoked; resulting in a lower mesh resolution requirement based on the turbulence model used to accurately predict flow features at this region.

1. Turbulence modeling.

The RANS method requires empirically developed turbulence models to predict the unstable flow features. Two two-equation turbulence models were tested; the Realizable $k-\varepsilon$ model[9] and the $k-\omega$ SST model[9]. The Realizable $k-\varepsilon$ model is deemed to be more accurate than the standard $k-\varepsilon$ model and it was tested due to its computational economy. The SST model is known for its robustness and accuracy in many general flow features especially due to its dual formulation of $k-\varepsilon$(in far field) and $k-\omega$(in boundary layer). However, for the steady-state RANS, a truly converged solution was only possible with the Realizable $k-\varepsilon$ model as the use of other turbulence model battled to maintain stability as the inherent nature of the flow is unsteady. Hence the results for the converged solution are presented here. The URANS result presented in this paper is the one with $k-\omega$ SST turbulence model as it was found to provide an overall better prediction compared to the Realizable $k-\varepsilon$ model. On the other hand, when the DES method was employed the one-equation Spalart Allmaras turbulence model was used due to is common use in industry[2] and more economical computational cost.

2. Spatial Discretization

Second order upwind discretization was used for all solution variables in the RANS method. The bounded central differencing scheme was used for momentum discretization for the LES and DES simulation as this was the suggested formulation to be used with these methods.[9] For similar reasons, the DES' modified turbulent viscosity was discretized using the bounded central differencing scheme. The SGS model used for the LES simulation was the Wall-Adapting Local Eddy-Viscosity (WALE) model due to its correct wall asymptotic (y^3) behaviour for wall bounded flows.[9]

3. Transient Formulation Temporal Discretization

The second order implicit time integration method was used for all simulations methods. This is because the explicit method is restricted by the Courant-Friedrichs-Lewy (CFL) condition which then restricts the time step selection. The timesteps for the present work was chosen based on a value that could provide a convergence down to three orders of magnitude. Salati[8] who did similar work, conducted Fast Fourier Transform (FFT) frequency analysis to determine suitable timesteps for transient solution methods. He conducted this analysis to determine the different dominant vortices that were captured with changing timesteps. The frequency analysis conducted for the three

different simulations methods are discussed in subsequent sections. Simulations conducted using the coarse and fine mesh were carried out at a timestep of 0.00025s and 0.0001s, respectively. The fine mesh was only tested for the LES simulation and based on the CGI obtained, other methods were not tested using the fine mesh as an immense amount of computational cost will be incurred with very small effect on the accuracy of the solution..

IV. Result

A. Midsurface coefficient of pressure

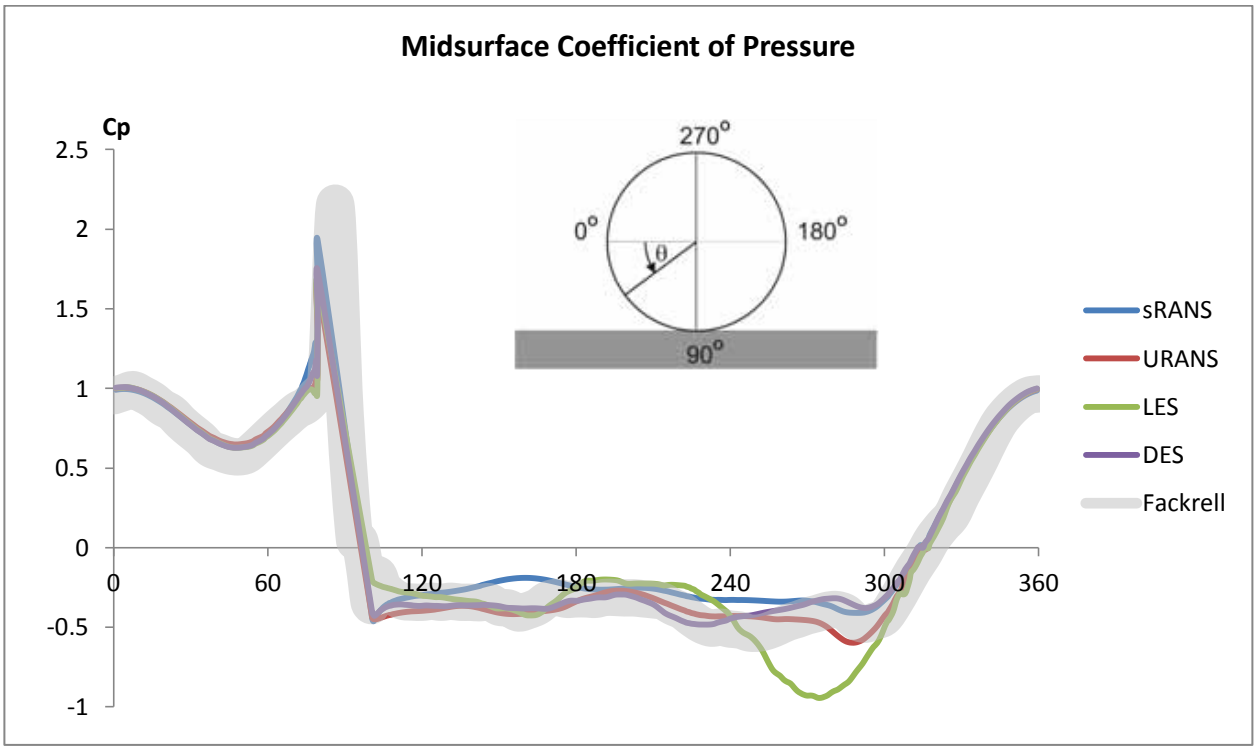

Figure 3. Midsurface time-averaged pressure coefficient

In Fig. 3, the semi-transparent thick grey line represents Fackrell's experimental result with errors associated with the readings he obtained.[3] Fackrell mentioned that the lift and drag results he obtained has a 5% error and since he derived these values by integrating the coefficient of pressure, the thick line represents the upper and lower bound for all his result that will account for a +-2.5% change in area under the graph.

Fackrell obtained the maximum pressure coefficient of 2.2 at the contact patch (90°). It can be seen that every simulation method under-predicted the peak pressure coefficient. The URANS, LES and DES methods predicted the peak C_p values to be 1.63, 1.66 and 1.73 respectively. McManus and Zhang[2] obtained values 36% higher than Fackrell in their URANS simulation using Realizable $k-\varepsilon$ turbulence model and Salati[8] obtained a 48% under predicted peak C_p value using the SST model. The accuracy of the prediction in this region is highly dependent on the geometry of the contact patch and the grid resolution. It is also obvious that the pressure peak is predicted to occur earlier at around 79°. This is due to the contact patch geometry that prohibited the location of the pressure peak to be accurately predicted.

The C_p values at the region behind the wheel, 90° to about 240°, were very well predicted by all simulation methods. Variation in prediction is most distinct at the separation region. Fackrell obtained result that indicated that separation occurs at a location between 280° to 290° with a C_p value of approximately -0.5. The steady-state RANS model predicted separation to occur at 290° and a corresponding C_p value of -0.41. Separation was predicted to occur at 287° and 293°, with C_p values of -0.6 and -0.38 by the URANS with SST turbulence model and DES, respectively.

The LES's prediction is the most distinct at this region, not matching the experimental or any other simulation methods tested. The LES predicted a much later separation at 275° with a C_p value of -0.94. The notieceable variation in C_P values at the seperation point potentially highlights the shortcoming of LES that requires an extremely high grid resolution close to the wall boundary layer. Near the wall, what could be a defined as 'large' eddies could become relatively small and require a Reynolds number dependent solution.[9] As such, the DES model was developed to overcome this problem because at the boundary layer, the DES method uses the URANS formulation to predict the flow behaviour and based on the results obtained here, it is likely to be able to overcome the shortcomings of LES.

B. Lift and Drag Coefficient

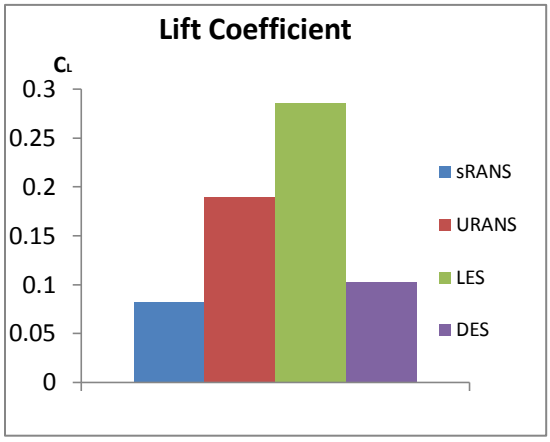

Figure 4. Time-averaged lift coefficient

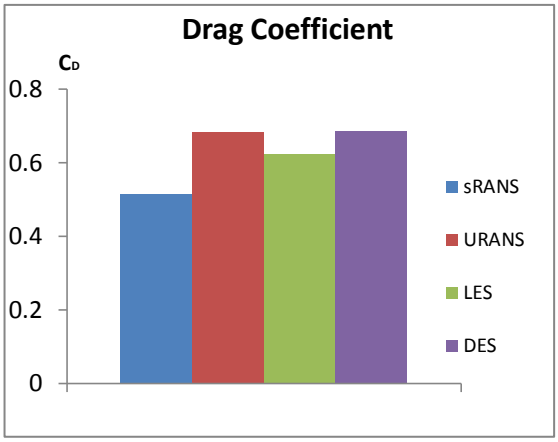

Figure 5. Time-averaged drag coefficient

Based on Fig. 5 it can be seen that the drag coefficient predicted by all transient simulation methods is relatively consistent. The lift coefficient shows distinct variations with different solution methods as shown in Fig. 4. The much later separation predicted by the LES could be causing the increased lift in its predictions. On the contrary, the earlier separation as predicted by DES and steady-state RANS compared to the URANS may have lead to the much lower pressure coefficient as postulated by Fackrell[3] and further confirmed by Diasinos[6].

C. Frequency Analysis

The lift and drag coefficient values on the wheel was obtained at every timestep. Then, this time domain function was converted to the frequency domain using the Fast Fourier Transform (FFT) algorithm in MATLAB. The frequency analysis could be used for a number of reasons in this context. Salati[8] used the frequency analysis to determine if there were any particular vortices that is being shed that influences the lift and drag value exclusively. He also used the frequency analysis to determine a suitable timestep for his transient simulations by observing if by changing the timestep were there any new,distinct vortices being shed that was predicted by the simulation (i.e. trying to obtain a timestep-independent solution).

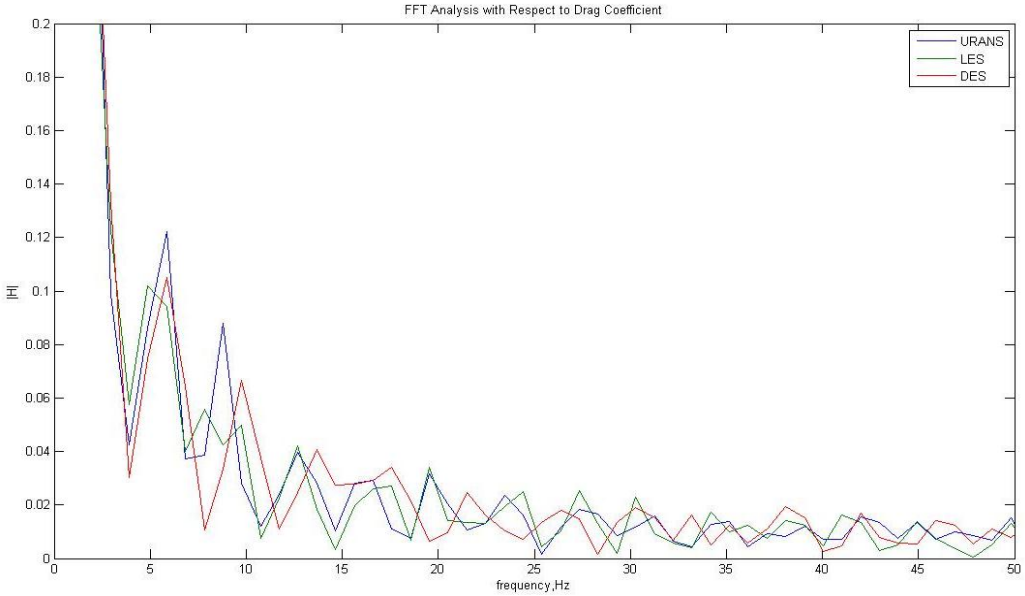

Figure 6. Frequency analysis based on drag coefficient

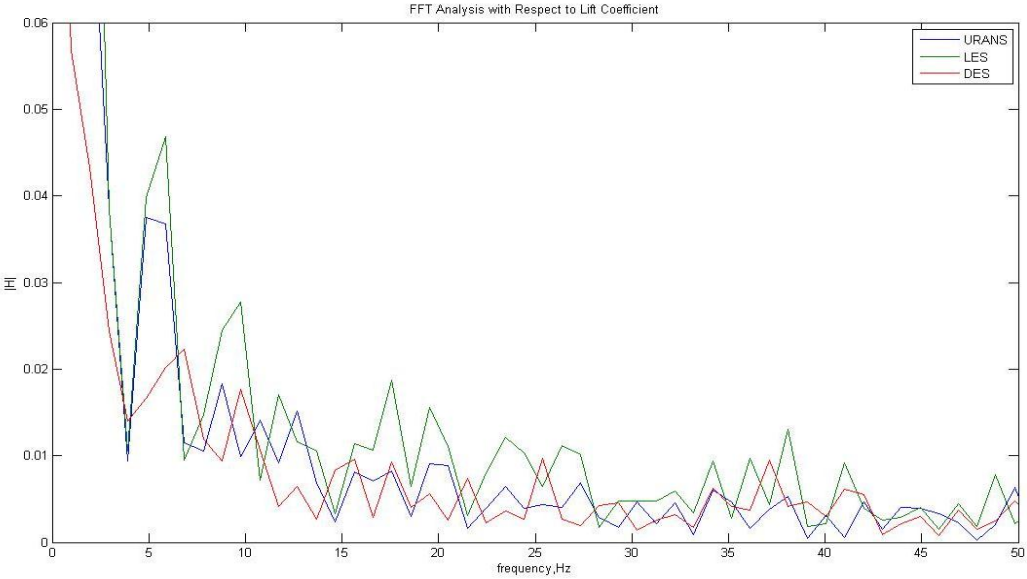

Figure 7. Frequency analysis based on lift coefficient

Based on the frequency analysis carried out for the present research most of the frequencies that influence the drag coefficient also influenced the lift coefficient significantly, indicating a strong coupling of the coefficients with regards to the vortex behaviour. From Fig. 6 and Fig. 7 these common frequencies are observed in all simulation methods in the region between 0 to 15Hz. Consequently, it can be concluded that there were no particular vortices that were exclusively determining the drag or the lift forces acting on the wheel , however the flowfield analysis in the following section indicates that the hub vortex exerts dominance.

The LES model has captured more vortices that is being shed as evident from the greater number of dominant peaks and troughs observed for frequencies below 15Hz in Fig. 6 and Fig. 7. All simulation methods were able to capture dominant frequency of about 4Hz, 6Hz ,7Hz and 10Hz. Hence, it shows that the choice of simulation methods may affect the prediction behaviour quite significantly, as even small changes in frequency for any particular vortex can influence the behaviour of the entire flowfield.

D. Flowfield Analysis

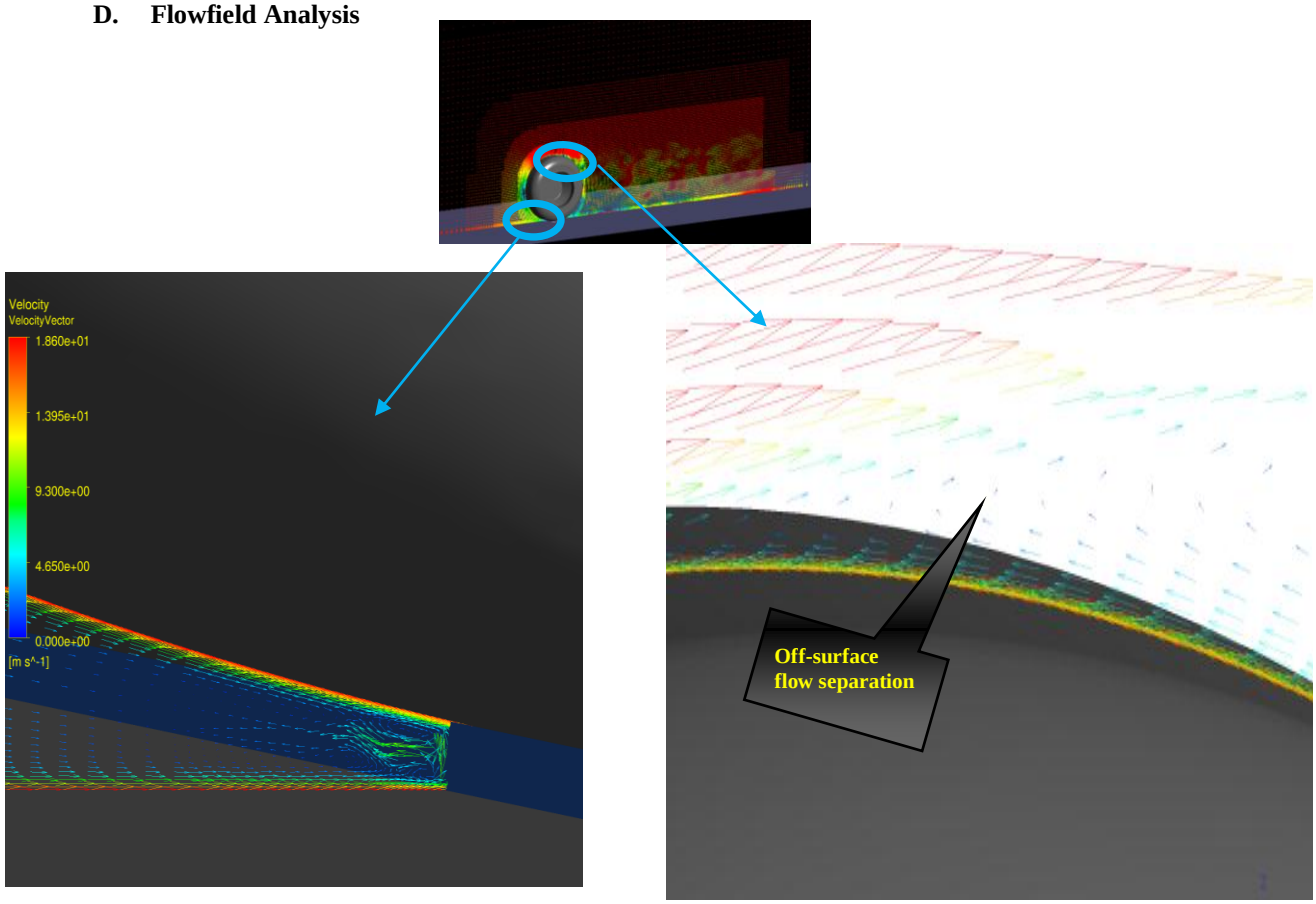

Figure 8. Velocity vector plot showing jetting effect adjacent to the contact patch (left) and off-surface flow separation (right)

A unique feature that Fackrell postulated for a rotating wheel was the jetting effect that occurred adjacent to the contact patch of the wheel.[3] Wind tunnel experiment would not have been able to show this effect unless expensive flow visualization techniques were used. However, in CFD, Fackrell's suggestion is demonstrated with clear visualization of the jetting effect occurring adjacent to the contact patch as shown in the left of Fig. 8.

Fackrell was able to mathematically prove that flow separation for a rotating body occurs just adjacent to the surface and not from the surface itself, due to the boundary layer remaining attached at the surface while the strong shear flow above travels in the direction opposite to the spinning. He was not able to visualize this effect in the wind tunnel but once again using CFD, it can now be shown that it is in fact the case that the flow on a rotating body separates just above the surface of the body. In the right of Fig. 8, flow separation is evident from the reversal in the direction of the velocity vector off the wheel surface.

The midsurface coefficient of pressure enabled comparison with the experimental data. However, the focus of this paper is to investigate the difference associated by doing advanced transient CFD simulation instead of the conventional steady-state RANS solutions – the effect was expected to be most pronounced in the wheel hubs and wake region where vortices and strong separated shear regions are present. So, the following flow field analysis was conducted with vorticity plots taken at three different locations along the wheel to highlight the difference in prediction by the various methods tested as part of the present work. The planes are at a location x/d=0.22, x/d=-0.04 and x/d=-0.52 from the centre of the wheel surface where the positive value corresponds to a plane forwards of the centre of wheel. The location of these plane is shown graphically in Fig. 9.

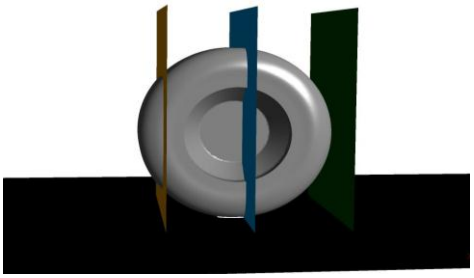

Figure 9. Planes used for result discussion of flow field. x/d=0.22(yellow),x/d=-0.04(blue) and x/d=-0.52(green)

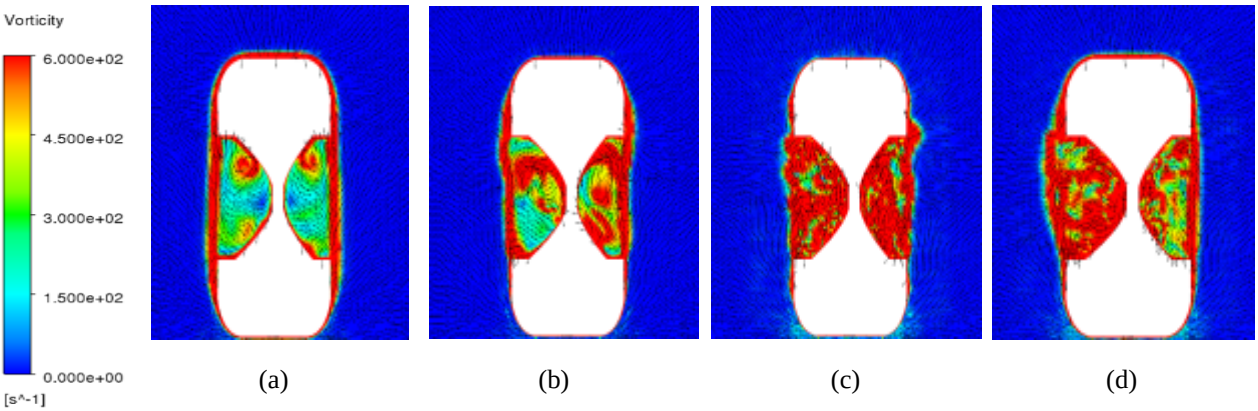

Figure 10. Vorticity plots at a plane x/d=0.22 for (a) Steady-state RANS (b) URANS (c) LES (d) DES

Figure 10 shows a plane taken at a location x/d=0.22 which is close to when the air just starts to flow into the hubs. In Fig. 10(a) the steady state RANS solution predicted a pair of upper wheel hub vortices. It is also important to note that this solution predicts similar flow behaviour between the right and left hub. The rest of the flow in the hubs is predicted to be unaffected with minimal flow swirling. The URANS solutions did not predict a upper wheel hub vortex being generated but a mid-hub vortex was generated as seen in Fig. 10(b). The flow pattern is dissimilar between the right and left hub and some more vigorous mixing is observed. However, the LES solution predicted the most amount of swirling and mixing occurring compared to any of the other solutions as shown in Fig. 10(c). Then, comparing the DES(Fig. 10(d)) solution to that of LES, at some locations in the hub, the URANS formulation has been invoked and different flow patterns are seen.

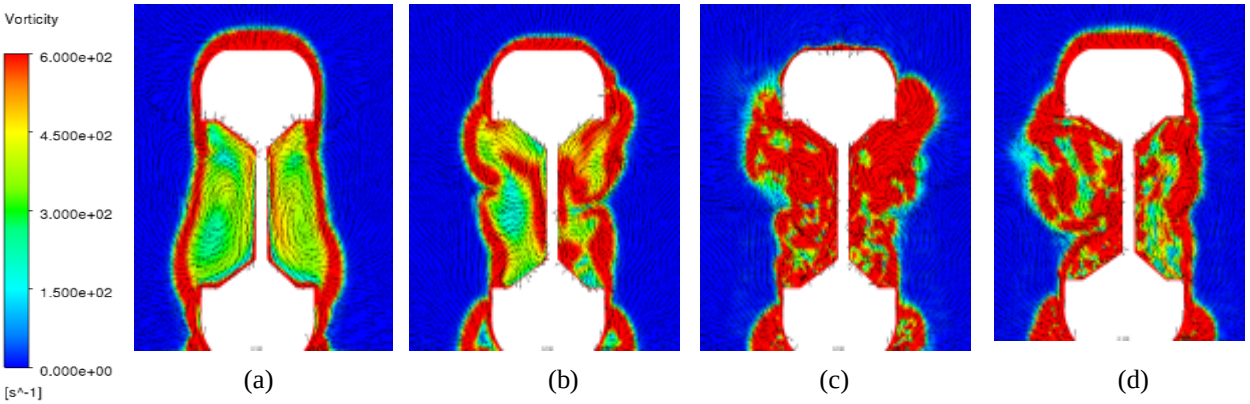

Figure 11. Vorticity plots at a plane x/d=-0.04 for (a) Steady-state RANS (b) URANS (c) LES (d) DES

Figure 11 shows a plane taken just slightly rearward of the wheel centreline at x/d=-0.04. Here, the flow has developed from when the flow first entered the hubs. It is obvious that the steady-state RANS solution predicted a very different overall flow feature compared to all the other simulations. The upper wheel vortex generated from the earlier plane have been pushed down to the mid-hub region to develop a pair of vortices in the lower hub region shown in Fig. 11(a). The URANS, LES and DES predicted the vortex from the mid-hub region to be pushed up to create a blowout effect as evident in Fig. 11 (b,c,d).The strongest blowout effect is predicted by the LES. The URANS approach predicts a cleaner flow inside the hubs. Another distinct variation is observed from the results of the steady-state RANS close to ground. Every other method predicted some increased level of activity in this region due to the dispersion of the flow that would have stagnated adjacent to the contact patch.

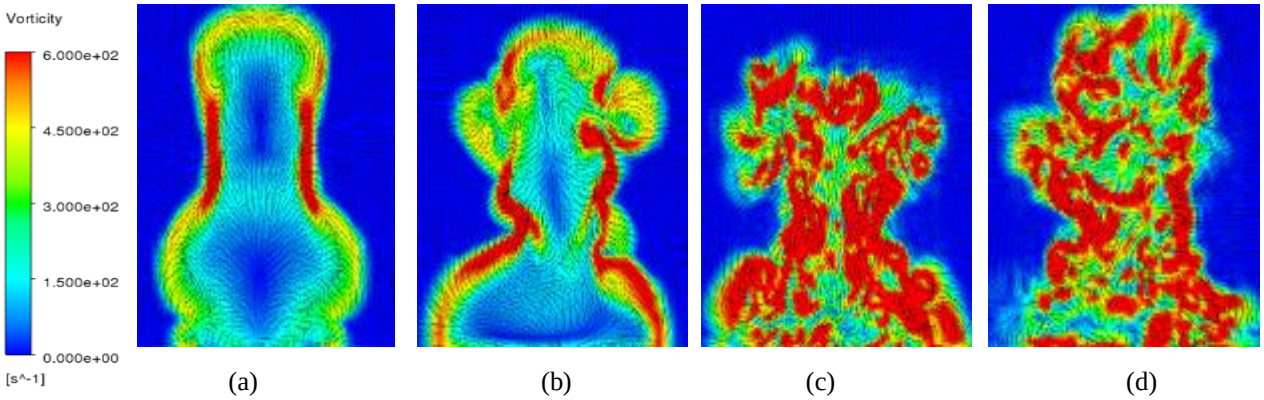

Figure 12. Vorticity plots at a plane x/d=-0.52 for (a) Steady-state RANS (b) URANS (c) LES (d) DES

Based on Fig. 12 it is obvious to note that there is no particular defined wake pattern that can be observed. Every method predicted a different wake structure and this is as expected since every method predicted the flow around the wheel and its hubs quite differently. The steady-state and unsteady RANS and DES predicted a taller wake compared to the LES's prediction. This could be attributed to the later separation predicted by LES. The deficiency of LES in correctly predicting the separation regions accounts for the different wheel wake height.

However, important flow features occur from the ground up. Around the region behind the contact patch, the steady RANS predicted a narrow wake structure as in Fig. 12(a) compared to a wide wake structure predicted by the other three methods. A wide structure is believed to be a better prediction as all the flow that stagnates forward of the contact patch would ideally spread out to the sides of the contact patch creating more disturbance in this region. LES predicts a pair to vortex close to the ground on both sides of the wheel. This vortex pair moves downstream and further analysis found that the more inboard vortex move higher up and further inboard whereas the outboard vortex keeps moving further outboard. The behaviour of the outboard vortex may not be ideal for aerodynamic performance of a F1 car as it may lead to losses due to disturbed air flow entering the floor of the car.

At the lower wake region, all simulation methods predicted a wide wake structure. If the wheel's geometry is extended to this region, the area covering the width of wheel is predicted to have very little swirling by the steady and unsteady RANS methods. The LES and DES shows that a lot of interaction is still taking place in this region. This is an important consideration since if a clean flow is predicted especially by the steady state RANS, it might provide false information about the flow behaviour because this lower wheel wake region will influence the performance of the under floor of a F1 car to generate downforce[10].

The mid-height wake region is predicted to be thinner by all the methods tested. The URANS, LES and DES provides evidence of a pair of vortex that is developed slight lower this region. These vortices moves downstream and have possible effect on the flow close to the sidepods in a F1 car. Using a steady RANS method, all this information is lost and the flow appears to be much cleaner than it actually is.

The upper wheel wake is affected by the blowout effect observed in the previous plane. Both URANS and LES predicted a wide upper wake region with LES predicting almost equally wide structure on both sides of the wheel. The DES did not predict an obviously wide wake structure as the blowout effect predicted was rather weak as

observed in Fig. 11(d). Again, here the deficiency of the steady-state RANS to not be able to predict the flow upstream correctly may provide inaccurate prediction at the wake. So, based on the findings of the present work, the steady-state RANS method may not only provide inadequate details of the flow but sometimes may also be quite inaccurate as such the flow is complex and evolves with time. In addition, the unsteady RANS approach did not provide a detailed enough interaction in the wake of the wheel which, by the prediction of LES and DES suggest to be more intricate.

V. Conclusion

The wake region is an important region of interest for aerodynamic performance in a F1 car. The unsteady disturbance at the lower wheel wake will affect the flow entering the floor of the car which works to generate a significant amount of downforce. Additionally, the upper wheel wake will meet the sidepods of the F1 car and affect the flow in this area. The investigations carried out in the present work have proven the need to model the flow over an exposed rotating wheel using advanced transient formulation to fully understand the flow structures. The RANS approach is robust in providing the general flow patterns but based on the results presented here, a lot of intricate flow details at the wheel wake seems to have been diffused. The LES and DES on the other hand are able to show more physical flow features that are expected to be occurring in real life. However, the computational cost involved in doing an advanced transient analysis like LES is immense and may deter industry application. The present work LES and DES were solved using a single node of 48 processors and took about 3-4 weeks of running time to obtain satisfactory results to do time-averaging. In addition, in this paper the deficiency of LES in the boundary layer region has been apparent with over-prediction of flow features in this region. It can be concluded that the DES is able to solve the shortcomings of LES very well.

VI. References

[1] Agathangelou, B. and M. Gascoyne, "Aerodynamic Design Considerations of a Formula 1 Racing Car," Society of Automotive Engineers, Inc. , 1998,980399.

[2] McManus, J. and X. Zhang, "A Computational Study of the Flow Around an Isolated Wheel in Contact With the Ground." Journal of Fluid Engineering, 2006. 128: p. 520-530.

[3] Fackrell, J. E., "The Aerodynamics of an Isolated Wheel Rotating in Contact With the Ground," Ph. D Thesis, Imperial College London(University of London),1974.

[4] Thom, A, "Experiments on the flow past a rotating cylinder", A.R.C R & M, 1931.

[5] Axon, L., "The Aerodynamic Characteristics of Automobile Wheels-CFD Prediction and Wind Tunnel Experiment," Ph.D Thesis,*College of Aeronautics*, Cranfield University, United Kingdom,1999.

[6] Diasinos, S., "The Aerodynamic Interaction of a Rotating Wheel and a Downforce Producing Wing in Ground Effect," Phd, School of Mechanical and Manufacturing Engineering, University of New South Wales, 2009.

[7] CD-adapco, *USER GUIDE: STAR-CCM+ Version 6.06.011*, 2011.

[8] Salati, L., "Detached Eddies Simulations on a fully exposed rotating wheel in contact with a moving ground," MSc Thesis, School of Mechanical and Manufacturing Engineering, University of New South Wales, Sydney, Australia, and Politecnico di Milano, Milan, Italy, 2012.

[9] ANSYS Inc, *FLUENT Theory Guide*, 2011.

[10] Ramachandran, D., "Complex Flow around an Exposed Rotating Wheel," B.Eng Thesis, School of Mechanical and Manufacturing Engineering, University of New South Wales, 2012.

[11] Morelli, A., "Aerodynamic Effect on an Automobile Wheel", MIRA Translation number 47/69 of A.T.A. p. 281-288, 1969.

[12] Stapleford, W.R. and G.W. Carr, "Aerodynamic Characteristics of Exposed Rotating Wheels", MIRA Technical Report, 1970.

[13] P.R.K. Dassanayake, D. Ramachandran, L. Salati , T.J. Barber, G.C. Doig, "Unsteady computational simulation of the flow structure of an isolated wheel in contact with the ground", 18th Australasian Fluid Mechanics Conference (AFMC), Australasian Fluid Mechanics Society (AFMS), Lauceston, Australia (submitted for publication)

[14] Zhang,X., Toet,W., Zerihan,J., "Ground Effect Aerodynamics of Race Cars," Applied Mechanics Reviews, Vol. 59, American Society of Mechanical Engineers (ASME),2006,pp. 33-48